

Research Article www.acsami.org

Electropolymerized Molecularly Imprinted Polymer Synthesis Guided by an Integrated Data-Driven Framework for Cortisol Detection

Grace Dykstra, Benjamin Reynolds, Riley Smith, Kai Zhou,* and Yixin Liu*



Cite This: ACS Appl. Mater. Interfaces 2022, 14, 25972-25983



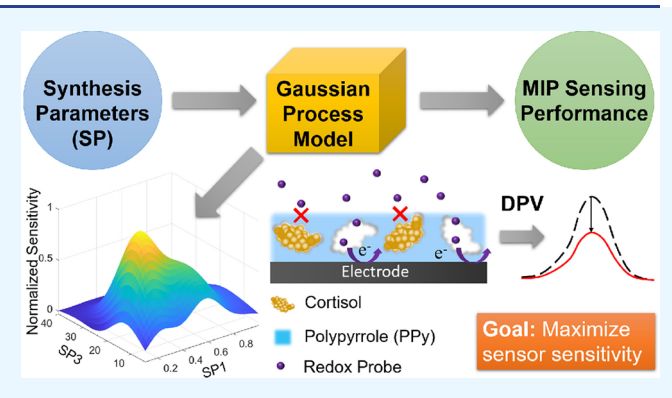
ACCESS I

Metrics & More

Article Recommendations

Supporting Information

ABSTRACT: Molecularly imprinted polymers (MIPs), often called "synthetic antibodies", are highly attractive as artificial receptors with tailored biomolecular recognition to construct biosensors. Electropolymerization is a fast and facile method to directly synthesize MIP sensing elements in situ on the working electrode, enabling ultra-low-cost and easy-to-manufacture electrochemical biosensors. However, due to the high dimensional design space of electropolymerized MIPs (e-MIPs), the development of e-MIPs is challenging and lengthy based on trial and error without proper guidelines. Leveraging machine learning techniques in building the quantitative relationship between synthesis parameters and corresponding sensing performance, e-MIPs' development and optimization can be facilitated. We herein demonstrate a case study



on the synthesis of cortisol-imprinted polypyrrole for cortisol detection, where e-MIPs are fabricated with 72 sets of synthesis parameters with replicates. Their sensing performances are measured using a 12-channel potentiostat to construct the subsequent data-driven framework. The Gaussian process (GP) is employed as the mainstay of the integrated framework, which can account for various uncertainties in the synthesis and measurements. The Sobol index-based global sensitivity is then performed upon the GP surrogate model to elucidate the impact of e-MIPs' synthesis parameters on sensing performance and interrelations among parameters. Based on the prediction of the established GP model and local sensitivity analysis, synthesis parameters are optimized and validated by experiment, which leads to remarkable sensing performance enhancement (1.5-fold increase in sensitivity). The proposed framework is novel in biosensor development, which is expandable and also generally applicable to the development of other sensing materials.

KEYWORDS: molecularly imprinted polymers, cortisol sensing, machine learning, Gaussian process, sensitivity analysis, synthesis optimization

1. INTRODUCTION

Molecularly imprinted polymers (MIPs) with tailored biomolecular recognition hold great promise to substitute antibodies used in biosensors and bioassays, which have clear advantages of low cost, easy fabrication, good stability, excellent durability, and long lifetime. 1,2 MIPs are synthetic receptors that mimic the "lock and key" mechanism in the natural biological antigen-antibody system. Traditionally, they are synthesized by polymerizing functional monomers, crosslinkers, and initiator molecules in the presence of a chosen "template" followed by a subsequent template removal process, which creates cavities with selective binding affinity to the template molecules.³ MIPs synthesized by bulk polymerization often suffer from deeply embedded cavities and poor transduction efficiency, leading to incomplete removal of template molecules, slow binding kinetics, and limited sensitivity.4 Electropolymerization emerges as a highly appealing method to synthesize MIPs as the recognition

element for electrochemical sensors. It is a fast and facile approach to directly construct MIPs in situ on the electrode's surface without cross-linkers and further electrode integration or immobilization. It is a highly controllable synthesis process with improved device-to-device reproducibility and real-time monitoring capability of polymer growth.5

Though synthesizing electropolymerized MIPs (e-MIPs) is a simple process, the rational design of e-MIPs for electrochemical sensors remains a challenge. There are two essential parts in the design of e-MIPs-based electrochemical sensors to

Received: February 10, 2022 Accepted: April 28, 2022 Published: May 10, 2022





achieve desired sensing performance: (1) selection of functional monomers that provide good interactions with the target analyte, (2) optimization of synthesis parameters, which control not only the formation, accessibility, and recognition capability of imprinted cavities, but also the transduction efficiency that turns the binding events to a measurable electrochemical signal. For example, cyclic voltammetry (CV) is a common method for electropolymerization, which offers good control of polymer growth. The number of electropolymerization cycles, applied voltage range, scan rate, ratio/ concentration of monomer/template, solvents, and supporting electrolytes all affect polymer film's thickness and morphology, which dictate the imprinting efficiency and sensing performance. While computational methods have been explored for monomer selection by calculating the monomer/oligomeranalyte binding energies, 6,7 the optimization process heavily relies on trial and error experiments without proper guidelines. Current optimization processes are mainly based on univariate methods, i.e., varying a single parameter with others being fixed. Prior knowledge is required to ensure that the initial values of parameters selected are in the vicinity of the optimal zone; otherwise, a blind search may take numerous iterations and not necessarily lead to an optimal recipe. In addition, the intrinsic correlation between synthesis parameters and sensing performance is often poorly understood, and the couplings among parameters are rarely captured. The conventional design-of-experiment (DOE) method is also challenging to implement due to the high dimensionality of the design space, which requires an exponentially increasing number of trials with an increasing number of factors and their levels. For example, a full factorial design of 5 factors with 3 levels results in 35 (243) runs plus replication, which is vastly timeconsuming and labor-intensive.

Along with the advancement of computational power, machine learning techniques have become the mainstream to facilitate various engineering applications through data-driven surrogate modeling (or metamodeling), including but not limited to drug discovery,8 molecular chemistry,9 and material science. 10 As the generation of experimental data in material science is often costly and time-consuming, most of the studies develop surrogate models based on the computational data or experimental data through text mining and data curation from the literature, 11-13 which allows a sufficiently large amount of data to construct the surrogate model with high performance. More recently, high-throughput experimental platforms have been integrated with machine learning to develop new materials and optimize synthesis to achieve desired properties. 14-16 However, when it comes to sensing materials, the sensing performance depends on not only the materials' intrinsic properties that can be directly measured but also materials' interactions with analytes and signal transduction. Therefore, the problem intrinsically is more complex, requiring additional steps to quantify their performance effectively and robustly. In this research, we employed a parallel 12-channel potentiostat coupled with low-cost screen-printed carbon electrodes (SPCEs) to synthesize e-MIPs and measure their electrochemical performance, which efficiently generates experimental data and ensures good reproducibility. SPCEs offer great convenience, efficiency, and cost-effectiveness to synthesize a large number of electrodes in different conditions and replication with minimum human handling to reduce labor cost and human-introduced variations. Nevertheless, the data set acquired from experiments still is of small size. While there

indeed exist a few previous studies that have achieved a certain level of success in establishing surrogate models using small-sized data sets, ¹⁷ the challenge of data scarcity remains open, depending on the target problem to be investigated.

In this research, we propose a systematic approach to optimizing e-MIPs synthesis for electrochemical sensing applications. This study is novel, as no one has reported integrating the tailored machine learning approaches in the sensing material design to guide material synthesis and optimize sensor performance. Specifically, a unified data-driven framework/platform was established upon the small-sized experimental data. The mainstay of this framework is a surrogate model, upon which tailored data analytics methods can be further employed to quantify the relationship between synthesis parameters of e-MIPs and resulting sensing performances, thereby providing guidelines for e-MIPs synthesis. As a proof-of-concept, cortisol (template)-pyrrole (monomer) system is selected in this research due to the following reasons: (1) cortisol, popularly called "stress hormone", is a highly valuable biomarker to be measured for stress management and personalized health monitoring, 18 (2) pyrrole is a widely used monomer for electropolymerization, and computational studies show that pyrrole can form more specific and stronger interaction with cortisol than other interfering steroid hormones (e.g., progesterone, prednisolone), 19 (3) overoxidation of imprinted polypyrrole (PPy) can be used to extract cortisol from the polymer matrix, 20,21 which is more controllable and repeatable than other chemical removal methods. While there are various surrogate models available for elucidating the causative relation of input and output in the experimental data set, in this research, we used the Gaussian process (GP) because it is intrinsically probabilistic that it is capable of accounting for the effects of inevitable measurement variations and synthesis uncertainties when performing model training and prediction. 22,23 This tightly aligns with the stochastic nature of real-world problems. The probabilistic decision-making enabled by GP appears to be robust, especially when the experimental data is small in size and subject to various uncertainty sources. In conjunction with the well-established GP, different sensitivity analyses were incorporated to elucidate the importance of e-MIPs' synthesis parameters and explore optimal recipes for e-MIPs synthesis.

2. MATERIALS AND EXPERIMENTAL DETAILS

2.1. Chemicals and Instrumentation. Potassium chloride, hydrocortisone, potassium (III) ferricyanide, potassium hexacyanoferrate (II) trihydrate, phosphate-buffered saline (PBS) tablets (1 M, pH = 7.4) were purchased from Sigma-Aldrich (St. Louis, MO, USA). Sulfuric acid (98%) was purchased from Fisher Scientific (Hampton, NH, USA). Pyrrole (99%) was purchased from Acros Organics (Fairlawn, NJ, USA). TE100 - RI Screen Printed Carbon Electrodes (SPCE) featuring a carbon working electrode (3 mm diameter), a carbon counter electrode, and an Ag/AgCl reference electrode were purchased from Zensor (Taichung City, Taiwan, ROC). Electrochemical measurements were taken using a PalmSens EmStat3, a 12-channel potentiostat (GA Houten, Netherlands). A Hitachi S-4700 field emission scanning electron microscope (FESEM) was used to acquire the SEM images.

2.2. Synthesis of e-MIP-Based Cortisol Sensors. The screenprinted carbon electrodes (SPCE), consisting of a carbon working electrode (3 mm diameter), a carbon counter electrode, and an Ag/AgCl reference electrode, were washed with 0.5 M H₂SO₄ by cycling the potential from -1.5 to 1.5 V for 10 cycles at a scan rate of 100 mV/s. The electrodes were rinsed with deionized water and left to dry at room temperature. All MIP films were synthesized by electro-

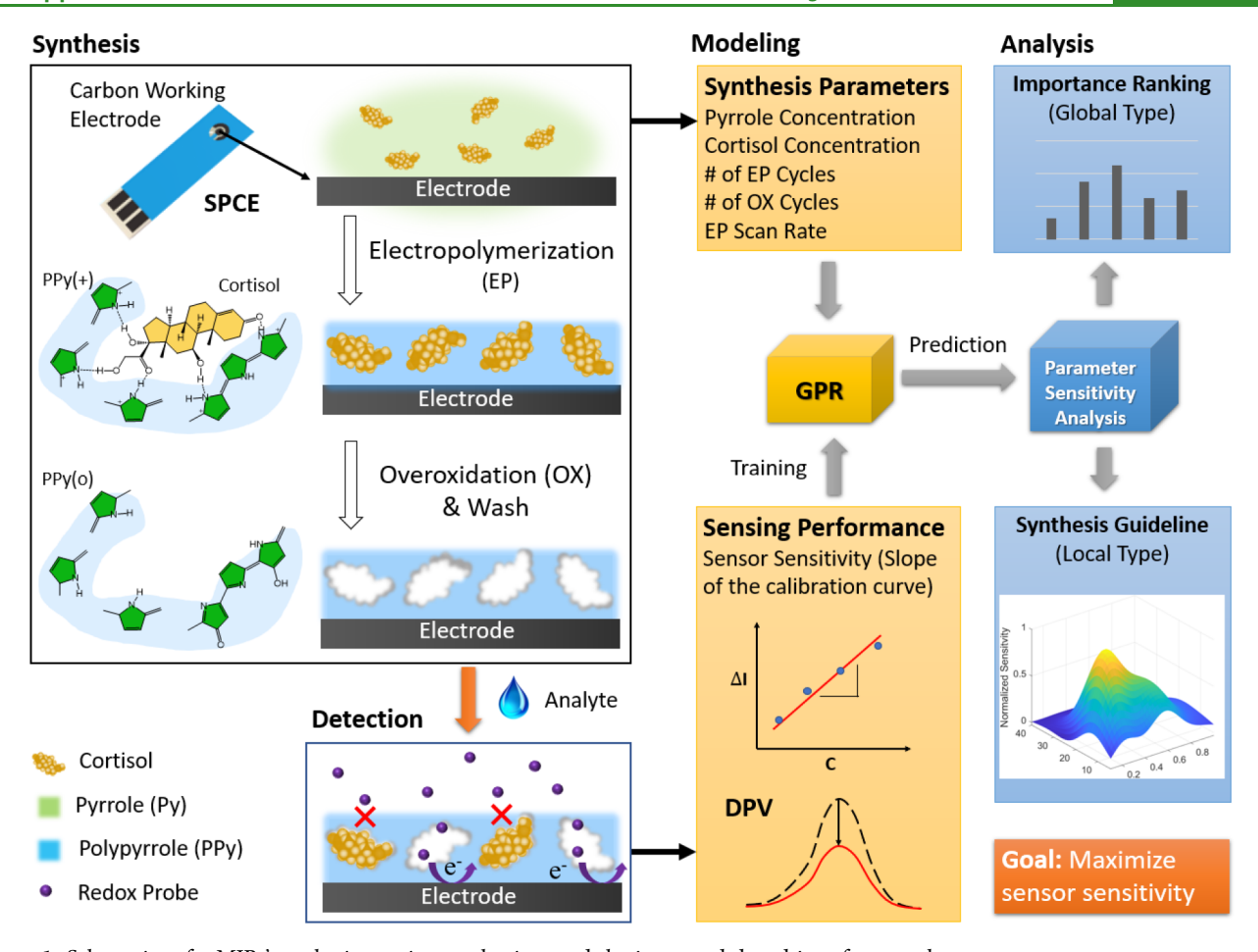


Figure 1. Schematics of e-MIPs' synthesis, sensing mechanism, and the integrated data-driven framework.

polymerization using CV at -0.2 to +0.9 V potential range. The polymerization solutions were prepared in 10 mM PBS (pH = 7.4) with 0.1 M KCl and various concentrations of pyrrole and cortisol. The number of polymerization CV cycles and the scan rate were parameters to be tuned. After the electropolymerization process, electrodes were rinsed with 10 mM PBS followed by overoxidation of PPy to extract cortisol from the polymer matrix. Overoxidation was carried out by CV at the potential range from -0.2 to +0.8 V in 10 mM PBS at a scan rate of 50 mV/s. The number of overoxidation CV cycles is a tunable parameter. After overoxidation, all electrodes were rinsed immediately with 10 mM PBS and left to dry at room temperature. Non-imprinted polymers (NIPs) were prepared following the same electropolymerization procedure and overoxidation without cortisol in the polymerization solution.

2.3. Sensor Electrochemical Characterization and Performance Evaluation. All sensors are subject to CV and a subsequent DPV in 80 μ L blank solution containing 10 mM PBS (pH 7.4) and 5 mM [Fe(CN)₆]^{3-/4-} as the redox probe. The electrochemical detection was carried out by placing 5 μ L of appropriate concentrations of cortisol solution at the working electrode for 15 min. 80 μ L PBS solution with 5 mM [Fe(CN)₆]^{3-/4-} was added to the working electrode after incubation. The measurements were performed using DPV at room temperature in the potential range of -0.10 to +0.35 V under the following conditions: pulse amplitude: 50 mV; pulse width: 50 ms; pulse time: 0.05 s; and scan rate: 10 mV/s.

3. RESULTS AND DISCUSSION

3.1. Overview of e-MIPs' Sensing Mechanism and Synthesis Framework for Cortisol Detection. e-MIPs-based cortisol sensors were fabricated on screen-printed carbon electrodes (SPCE) by electropolymerization of pyrrole in the

presence of cortisol molecules and subsequent overoxidation of polypyrrole (PPy) to extract cortisol from the PPy matrix, as illustrated in Figure 1. Cyclic voltammetry (CV) was employed for electropolymerization, where cortisol molecules get imprinted in the PPy matrix through hydrogen bonding. During overoxidation in PBS, hydroxyl (-OH), carbonyl (C= O), and carboxylic groups (COOH) are formed at the β positions of the pyrrole ring due to high potential, which lessen and weaken hydrogen bonding leading to cortisol elution.²¹ This process creates cavities structurally complementary to cortisol with sufficient binding affinity for the following cortisol sensing. A redox probe, ferro/ferricyanide ($[Fe(CN)_6]^{3-/4-}$), was used to signify the rebinding between cortisol molecules in the testing samples and the imprinted PPy. With cortisol molecules rebinding to imprinted PPy, the cavities were filled, which blocks the access of the redox probe to the electrode surface, thus reducing electron transfer resulting in a decreased electrochemical signal. Differential pulse voltammetry (DPV) was employed to quantify cortisol concentration in spiked samples, as it is an effective method to suppress electrochemical interferences and increase sensor sensitivity by eliminating the charging current.²⁴ The calibration curve can be established between cortisol concentrations and their corresponding peak current change of DPV curves (ΔI) , which is the metric to evaluate e-MIPs' sensing performance. The higher the slope of the calibration curve is, the more sensitive the sensor is to cortisol.

The sensing performance of e-MIPs-based cortisol sensors is governed by the synthesis parameters (SPs). Based on the

literature and prior experiments, the polymerization solution was prepared with 10 mM PBS using 0.1 M KCl as a supporting electrolyte. The CV potential range for electropolymerization was set from -0.2 to 0.9 V, and overoxidation was performed in 10 mM PBS by cycling potential from -0.2to 0.8 V at a fixed scan rate of 50 mV/s. Pyrrole concentration (SP1) and cortisol concentration (SP2) in the polymerization solution, the number of electropolymerization CV cycles (# of EP cycles, SP3), the number of overoxidation CV cycles (# of OX cycles, SP4), and the electropolymerization CV scan rate (EP scan rate, SP5) are five synthesis parameters that we investigated in our study. The samples of those synthesis parameters were purposely designed, and the corresponding sensing performances were then experimentally measured. Building upon the paired relations between synthesis parameters and measured sensor sensitivity, an integrated data-driven framework was established to comprehensively investigate the impact of e-MIPs' synthesis parameters on sensing performance. As shown in Figure 1, the GP surrogate model was built as the backbone of the framework. Once the GP surrogate model was well established via experimental data, its efficient and reliable predictions were fully leveraged to facilitate the subsequent global and local sensitivity analyses, aiming at quantifying the parameter importance and providing synthesis guidelines, respectively. The detailed results enabled by this synthesis framework are subsequently introduced.

3.2. Synthesis Parameter Sampling. The purpose of the experimental data acquisition is to guide the surrogate model establishment. The accuracy of the surrogate model usually hinges upon the size and quality of the available data set. While a data set with a large size certainly can ensure the high fidelity of the surrogate model, it substantially increases the data acquisition cost. In this research, there are five synthesis parameters involved, and their ranges are listed in Table 1

Table 1. Ranges of Synthesis Parameters (SP) Investigated

| | Pyrrole | Cortisol | # of EP | # of OX | EP Scan |
|-------|----------|----------|---------|---------|----------------|
| | Conc. | Conc. | Cycles | Cycles | Rate |
| | (SP1) | (SP2) | (SP3) | (SP4) | (SP5) |
| Range | 0.03-1 M | 1-20 mM | 4-40 | 5-40 | 10-100 mV/s |

(values of SP3, SP4, and SP5 are integers). Due to the high dimensionality of the design space, adopting the conventional design of experiment (DOE) that discretizes uniform grids given the bounds of parameters and retrieves samples from all possible parameter combinations will lead to a considerable size of samples. Therefore, without prior knowledge, we employed one space-filling sampling method, i.e., Latin hypercube sampling, to generate the first group of synthesis parameter samples from a multivariate uniform distribution given the prespecified ranges (Table 1).²⁵ For illustration, 32 generated samples in the first group are distributed in the lowdimensional space with the marker "Blue dots" shown in Figure 2. Consistent with the underlying idea of the Latin hypercube sampling method, the distribution yield is relatively uniform. It was found through the experimental testing that more than two-thirds of fabricated sensors did not show any CV or DPV peaks in the presence of $[Fe(CN)_6]^{3-/4}$ due to either a large number of electropolymerization cycles (# of EP cycles >20) or a large number of overoxidation cycles (# of OX cycles >20), yielding a sensor sensitivity of zero. As mentioned, sensor sensitivities are represented by the slope of the calibration curve, which is a continuous variable. Therefore, the surrogate model to be established essentially serves the regression analysis. In order to improve the accuracy of the surrogate model, more sensitive sensors are required to fill in the workable space. While the surrogate model built upon the first group of samples may not be adequately reliable for quantifying the relationship between synthesis parameters and sensor sensitivities over the entire space, it can be used to qualitatively guide additional synthesis parameter sampling toward working sensors, resulting in a second group of 40 samples of synthesis parameters marked with "Orange dots" in Figure 2. The entire data set combines samples produced in both groups, consisting of 72 samples of synthesis parameters and corresponding measured sensor sensitivities. As will be shown later, we will use this experimentally collected data set to construct the surrogate model instead of directly implementing the sensitivity analysis, because the data set is small-sized and prone to yield different results when adopting different metrics in a subjective manner.

3.3. Characterization of e-MIPs-Based Cortisol Sensors, Sensing Performance, and Sensor Reproducibility.

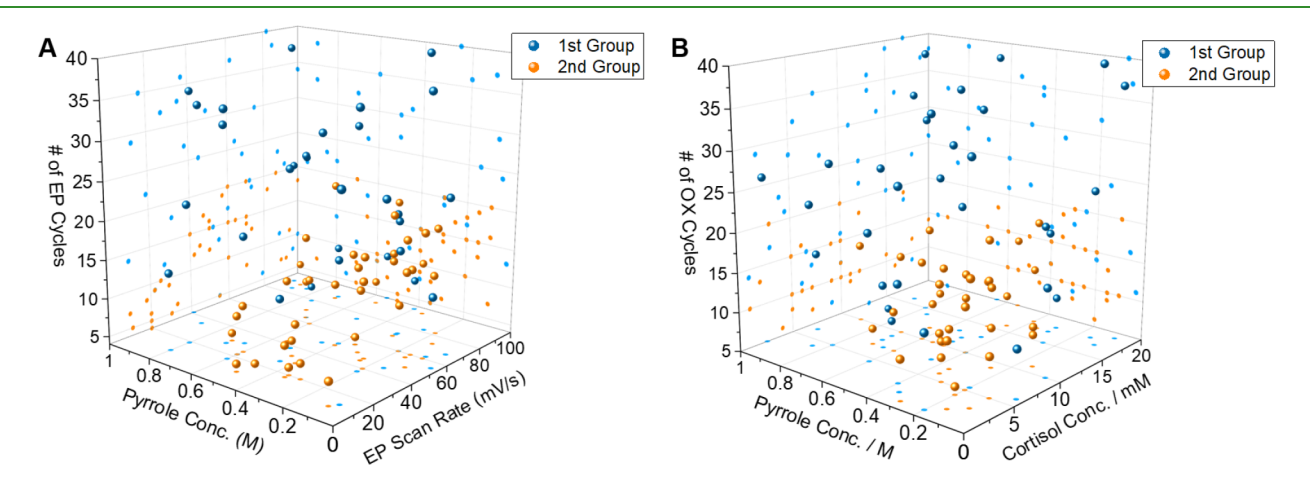


Figure 2. Three-dimensional illustration of the generated synthesis parameter samples from multivariate uniform distribution-based Latin hypercube sampling (first Group, Blue dots) and additional sampling (second Group, Orange dots) (A) SP1 versus SP3 versus SP5; (B) SP1 versus SP2 versus SP4.

Table 2. Input (Synthesis Parameters) and Output (Sensor Sensitivity) of Representative Samples

| | | | Input | | | Output | | |
|------------------------------|--------------|---------------------|----------------|----------------|--------------------|---|--------|----------|
| Sample Index ^a | Py Conc. (M) | Cortisol Conc. (mM) | # of EP Cycles | # of OX Cycles | $EP SR^{b} (mV/s)$ | Avg. Sensitivity $(\mu A/\log_{10}C)^c$ | SD^d | Category |
| 15 | 0.2 | 5 | 10 | 15 | 60 | 3.228 | 0.442 | 3 |
| 17 | 0.25 | 15 | 40 | 20 | 82 | 0 | 0 | 1 |
| 19 | 0.25 | 9 | 13 | 10 | 45 | 5.177 | 0.480 | 3 |
| 24 | 0.3 | 5 | 15 | 10 | 50 | 6.072 | 0.528 | 3 |
| 25 | 0.3 | 5 | 20 | 15 | 70 | 5.821 | 0.552 | 3 |
| 30 | 0.35 | 6 | 8 | 16 | 18 | 0 | 0 | 1 |
| 46 | 0.5 | 10 | 18 | 15 | 100 | 2.955 | 0.478 | 3 |
| 56 | 0.65 | 20 | 18 | 38 | 31 | 0 | 0 | 1 |
| 70 | 0.9 | 10 | 7 | 15 | 90 | 1.205 | 0.265 | 2 |

[&]quot;Sample index is sorted by pyrrole concentration in ascending order. ${}^{b}SR - Scan$ rate. ${}^{c}log_{10}C - log_{10}$ (cortisol concentration). ${}^{d}SD - Standard$ deviation.

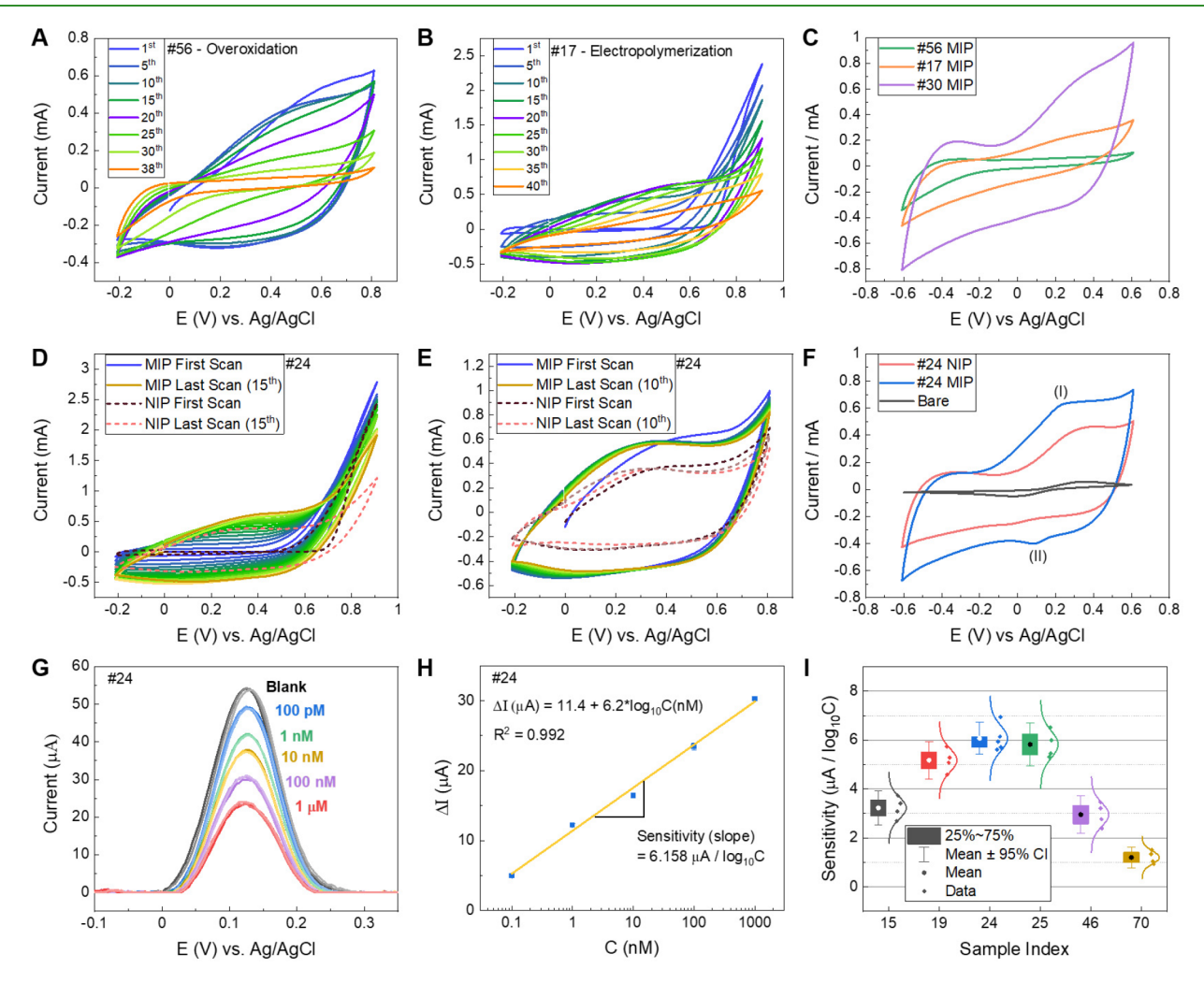


Figure 3. (A) Overoxidation cyclic voltammogram of sample #56. (B) Electropolymerization cyclic voltammogram of sample #17. (C) Cyclic voltammogram of sample #56 (green), #17 (red), and #30 (purple) in 10 mM PBS with 5 mM $[Fe(CN)_6]^{3-/4}$ at 50 mV/s. (D) Electropolymerization cyclic voltammogram of sample #24 and its corresponding NIP (no cortisol in polymerization). (E) Overoxidation cyclic voltammogram of sample #24 and its NIP. (F) Cyclic voltammogram of bare SPCE, sample #24, and its NIP in 10 mM PBS with 5 mM $[Fe(CN)_6]^{3-/4}$ at 50 mV/s. (G) DPV response of sample #24 to increasing cortisol concentration from 100 pM to 1 μ M in 10 mM PBS with 5 mM $[Fe(CN)_6]^{3-/4}$. (H) Calibration curve between DPV peak current response and logarithm of cortisol concentration with the linear regression equation. (I) Illustration of sensor reproducibility where multiple replicates were made. (Cl: confidence level).

For each set of synthesis parameters (one sample), cyclic voltammograms during the electropolymerization and over-oxidation process were recorded, which reflect the status of polymer growth and changes. After as-fabricated sensors were

dried overnight, CVs were carried out to characterize the redox behavior of $[Fe(CN)_6]^{3-/4}$ on e-MIPs-modified SPCEs, and DPV was conducted to quantify sensor sensitivity to cortisol in a series of spiked samples. There are three typical categories of

e-MIPs' electrochemical behaviors: (1) negligible or no DPV peaks, (2) clear DPV peaks, but peak value does not change or slightly reduces after introducing cortisol (sensor sensitivity less than 2 μ A per order of magnitude increase in cortisol concentration), (3) DPV peak noticeably decreases with increasing concentration of cortisol. The synthesis parameters of representative samples and their corresponding sensitivities are shown in Table 2.

For sensors in Category 1, a couple of scenarios can lead to negligible or no DPV peaks in the presence of a redox probe $([Fe(CN)_6]^{3-/4-})$. First of all, the extreme extent of overoxidation inserts carboxyl groups (COOH) and damages pyrrole rings, which dramatically reduces the conductivity of PPy and impedes electron transfer. 21 For illustration, the overoxidation voltammograms of an e-MIP-modified SPCE (sample index #56 with 38 overoxidation cycles) are shown in Figure 3A. One can notice that the cyclic voltammogram in each scan holds its shape relatively well until the 20th scan, and further overoxidation drastically changes the shape and reduces the polymer film's conductivity. The subsequent CV in the presence of [Fe(CN)₆]^{3-/4-} shows a very narrow voltammogram without redox peaks (Figure 3C (green)). While the sensors fabricated with different synthesis parameters have different voltammogram shapes after electropolymerization, the same trend was observed across the board after excessive overoxidation. Similar phenomena were also observed during the electropolymerization process with too many CV scans. For example, as shown in Figure 3B (sample index #17 with 40 electropolymerization cycles at a scan rate of 82 mV/s), the capacitive current during electropolymerization increases in each scan initially until the 20th scan, indicating controlled polymer growth. After the 25th scan, further CV scans result in decreased capacitive current, which can be ascribed to the termination of polymer growth and the start of overoxidation. Besides, PPy's growth also depends on the scan rate during electropolymerization. Slow scan rate usually yields a tighter and less porous film, ^{26,27} which completely blocks the access of the redox probe to the electrode surface, leading to no redox peaks in CV and DPV in the presence of $[Fe(CN)_6]^{3-/4}$. For a typical e-MIP fabricated with a slow scan rate (sample index #30 with 8 electropolymerization cycles at a scan rate of 18 mV/s), it preserves PPy's high capacitive current but does not show redox peaks of $[Fe(CN)_6]^{3-/4}$, as indicated in Figure 3C (purple). The complete synthesis voltammograms of samples #56, #17, and #30 are presented in Figure S1.

On the other hand, with few electropolymerization cycles, e-MIP film becomes too thin or loose so that redox probe has free access to electrode surface regardless of cortisol's presence, which results in prominent CV redox peaks and DPV peaks but a limited response to cortisol molecules (Category 2), as shown in Figure S2. Sensors in Category 1 usually have zero sensitivity, and sensors in Category 2 have a limited sensitivity of less than 2 μ A/log₁₀C. Only sensors in Category 3 are considered as working sensors.

For a typical working sensor, its corresponding non-imprinted polymer (NIP)-modified SPCE can be fabricated following the same electropolymerization and overoxidation procedure without adding cortisol in the polymerization solution. As an illustration, the synthesis, electrochemical characterization, and cortisol sensing performance of one of the best e-MIP-modified SPCEs (sample index #24) are shown in Figure 3D—H with comparison to its corresponding NIP. During electropolymerization, the capacitive current increases

in each scan, indicating the ongoing controlled formation of PPy. While the NIP electropolymerization shares the same voltammogram shape as MIP, its current is lower than that of MIP, implying that the binding of electro-inactive cortisol molecules increases the capacitive current of the PPy film (Figure 3D). Ten cycles of overoxidation of MIP and NIP in PBS maintains the voltammogram shape relatively well without jeopardizing PPy's conductivity, as shown in Figure 3E, indicating that the partially overoxidized PPy was obtained during the process. The electrochemical behavior of bare SPCE and MIP- and NIP-modified SPCE was investigated by CV in PBS in the presence of 5 mM $[Fe(CN)_6]^{3-/4}$. As shown in Figure 3F (gray), a couple of well-defined reversible redox peaks for the [Fe(CN)₆]^{3-/4-} redox probe were observed on bare SPCE with an anodic peak current of 60 μ A. The MIPmodified SPCE shows an increase in capacitive currents with a broad redox oxidation peak (I) and a reduction peak (II) as shown in Figure 3F (blue), whereas negligible redox peaks were observed on NIP-modified SPCE (Figure 3F (red)). Their SEM images are presented in Figure S3, which shows overall smaller NIP particles than MIP, indicating that pyrrole forms a more compact film without a cortisol template. DPVs were performed on MIP-modified SPCE to detect different concentrations of cortisol (Figure 3G) with 15 min incubation time, and a calibration curve can be established which shows a linear relationship between ΔI (change of DPV peak current: $\Delta I = I_{\text{Blank}} - I$) and the logarithm of cortisol concentration (log₁₀C), as shown in Figure 3H. The slope value, defined as sensor sensitivity, is used as the metric to evaluate sensing performance, serving as the output of the surrogate model.

As data quality and credibility are essential to establish a high-fidelity surrogate model, sensors were made in duplicate to ensure reproducibility. When the sensitivity values of the duplicates are close, the average is used as the output for this sample. Due to inevitable manufacturing variation, experimental uncertainties, and human handling variations, some duplicates show certain differences in measured sensitivity. In such cases, more sensors were fabricated using the same synthesis parameters for these samples, and the mean value of sensor sensitivities is used as the output. The statistical properties of measured sensor sensitivities of these samples are described using the box plot with fitted normal distributions, as shown in Figure 3I, and their detailed information is listed in Table 2. Overall, the result shows good reproducibility. Since the measurement is probabilistic in nature, a surrogate model that is capable of estimating the uncertainty effect and accordingly performing the decision making with confidence level is required. The synthesis parameters-sensitivity relations can be deemed as input-output relations to establish the surrogate model in the subsequent subsection.

3.4. Surrogate Model Establishment for Synthesis Parameters-Sensing Performance Correlation Characterization. In this subsection, the Gaussian process (GP) surrogate model is constructed on the experimentally acquired data set above. As mentioned, this surrogate model essentially is a regression model because of the continuous output of interest (sensor sensitivity). We hence can simply describe it as a Gaussian process regression (GPR) model. The mathematical formulation of GPR is presented in the Supporting Information, Note \$1.1. Generally, 72 samples are a small-sized data set, and the regular training—testing data split based on the specified ratio thus is no longer adequate for the systematic model validation purpose. To take full advantage of limited

data, here we adopt the leave-one-out cross validation, 28 in which the number of emulations required equals the number of samples, i.e., 72. In each emulation, 1 out of 72 samples is selected as the testing sample and the rest are training samples. In this context, leave-one-out cross validation is an extreme case of leave-p-out or k-fold cross validation. 28 In order to establish a reliable GPR model, the covariance function shown in Equation (S1) needs to be tuned in light of the crossvalidation performance. The covariance functions available for selection include those provided in Equation (S2) and their automatic relevance determination (ARD) forms. In this research, the best covariance function obtained via the crossvalidation-based grid search is the ARD squared exponential function. The hyperparameters in the covariance function are identified through Bayesian optimization-based model training. Figure S4 gives the training accuracy of 4 representative emulations. As highlighted in the Introduction, GPR is a probabilistic machine learning method, which can yield the probabilistic prediction result, i.e., prediction means and standard deviation. Note that the training data's output (sensor sensitivity) is normalized into the range [0,1] for training stability. Therefore, the normalized sensitivity is used for illustration throughout the manuscript unless otherwise specified. The actual training outputs and corresponding predicted outputs (i.e., prediction mean) have a good agreement. The 95% confidence interval (±2 standard deviations of mean) of predictions is also given in the result, which essentially represents a range where the actual value will fall in with 95% probability. The confidence interval usually becomes larger when the prediction error, i.e., the discrepancy between the prediction mean and actual measured sensitivity value, is more significant. It is found that the 95% confidence interval across the sample space generally is narrow, indicating the high confidence of predictions. The probabilistic result enabled by GPR essentially accounts for the uncertainties in prediction and hence can allow one to incorporate the judgment to further facilitate wise decision making. The results overall illustrate adequate model training even under a small-sized data set.

As mentioned, all samples will be consecutively tested at different emulations in the leave-one-out cross validation. The cross-validation result is shown in Figure 4. Compared with Figure S4, the same probabilistic feature in the result can be observed. While the testing errors between the predictions and

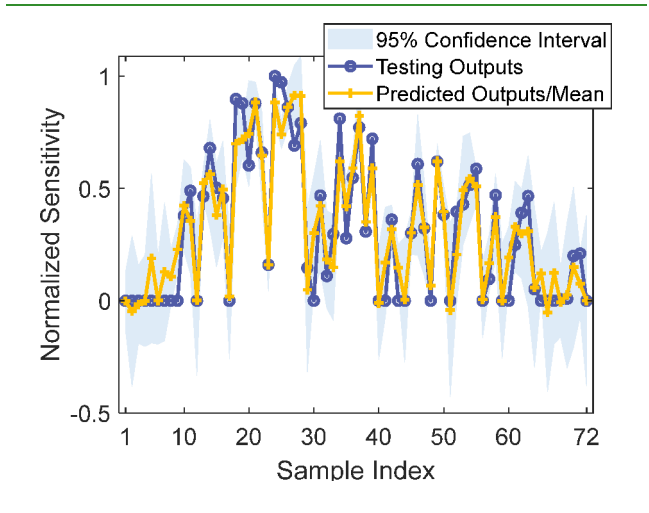


Figure 4. Leave-one-out cross-validation testing result.

actual values become slightly more noticeable than the training errors, and the confidence intervals expand accordingly, the predictions overall match well with the actual values.

In order to highlight the excellent performance of GPR under a small-sized data set, we involve other representative surrogate models for result comparison, including support vector regression (SVR),²⁹ decision tree (DT),³⁰ and multilayer perceptron (MLP) neural network (NN).31 Similar to GPR, those models have some parameters that cannot be directly optimized, which instead are subject to tuning. In this research, we consider kernel, tree depth, and node number in the hidden layer as the tunable parameters of SVR, DT, and NN, respectively. The same cross-validation analysis and grid search used above were carried out for all benchmark surrogate models. For illustration, the normalized mean squared error (NMSE) and coefficient of determination (also known as R squared) of all testing samples are utilized to assess the crossvalidation accuracy comprehensively, and the results are tabulated in Table 3. Clearly, given a small-sized data set,

Table 3. Comparison of Leave-One-out Cross-Validation Accuracy of Different Surrogate Models

| | GPR | SVR | DT | MLP-NN |
|------------|--------|--------|--------|--------|
| NMSE | 0.0120 | 0.0496 | 0.0364 | 0.0771 |
| R squareda | 0.8765 | 0.4877 | 0.6242 | 0.2038 |

^aNote: R squared value is closer to 1, the more accurate the result is.

GPR significantly outperforms other surrogate models in terms of cross-validation accuracy. The fundamental reasons for such improvement lie in the probabilistic learning strategy and configuration of GPR. Unlike the general regression models that minimize the mean squared error (MSE) during training, GP regression that fundamentally is built upon Bayesian inference³² aims at maximizing the likelihood estimation during training, which may perform more robustly under the data with the correlation that is contaminated by uncertainties. As shown in the Supporting Information, mathematically, the covariance kernel allows one to incorporate a hyperparameter to mimic the noise effect. Moreover, the different complicated forms of kernel functions available make GP adequately flexible and feasible to model various types of stochastic problems.

3.5. Investigation of Synthesis Parameter Impact to Facilitate e-MIPs Synthesis Optimization. 3.5.1. Sobol Index-Based Global Sensitivity Analysis for Synthesis Parameter Importance Ranking. In order to gain a profound understanding of the complex e-MIPs synthesis process, global sensitivity can be carried out to quantify the importance of synthesis parameters with respect to the sensing performance. In this research, we particularly use the Sobel index, because it can characterize the multivariate contribution, i.e., couplings of synthesis parameters, which elucidates the nature of the actual synthesis process. The mathematical formulation of this method is in the Supporting Information, Note S1.2. The Sobol index-based global sensitivity analysis is implemented through the Monte Carlo simulation, where each simulation run resorts to the well-established GPR for efficient sensitivity prediction. The total number of Sobol indices in this research is 31 (i.e., $2^5 - 1$), for each of which 20 000 Monte Carlo simulation runs are carried out to generate 20 000 paired input-output relations.

Over the entire design space constructed upon the parameter range specified in Table 1, Sobol indices with

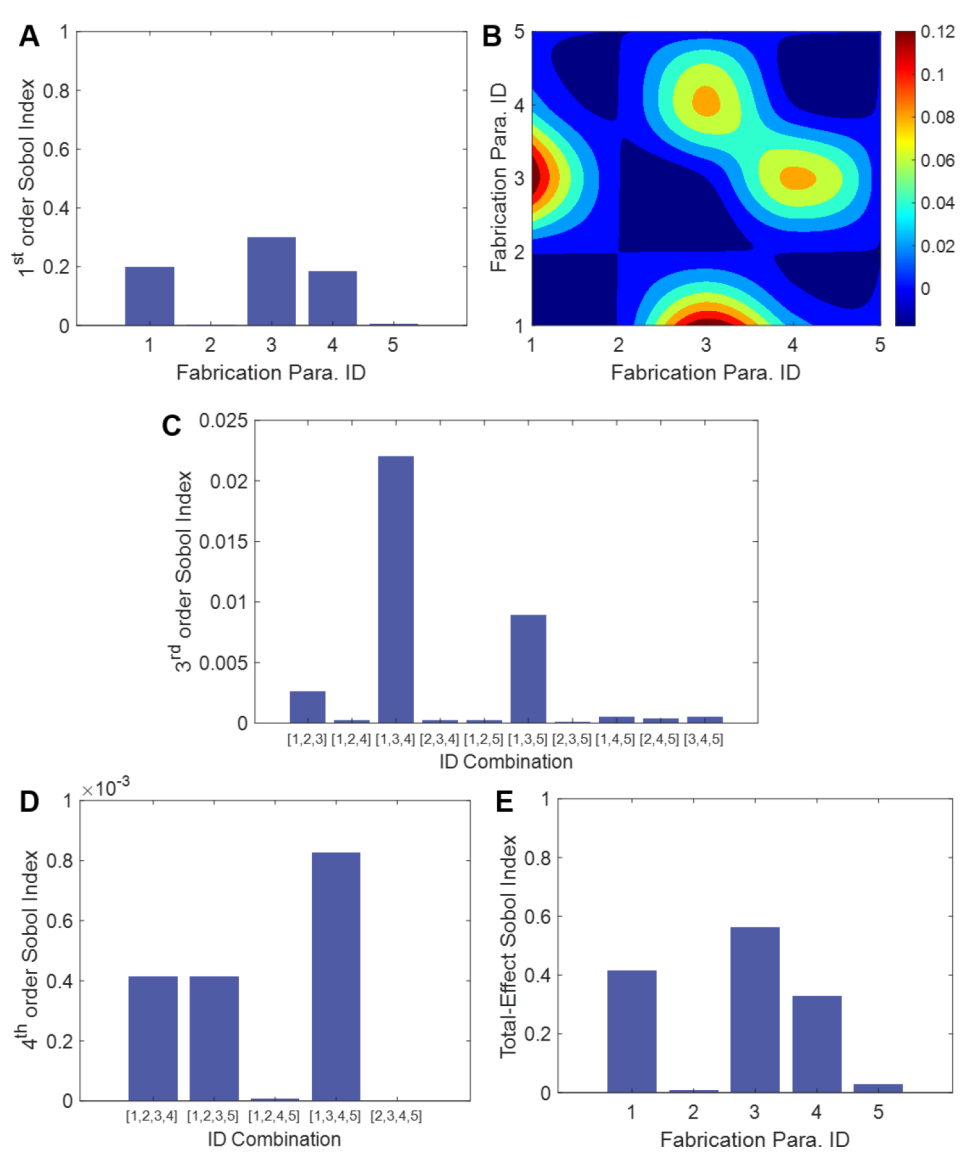


Figure 5. Importance quantification of synthesis parameters using Sobol indices with different orders over the original design space: (A) first-order Sobol index; (B) second-order Sobol index; (C) third-order Sobol index; (D) fourth-order Sobol index; (E) total-effect Sobol index (SP1: Pyrrole concentration (M); SP2: Cortisol concentration (mM); SP3: # of EP cycles; SP4: # of OX cycles; SP5: EP Scan rate (mV/s)).

different orders can be calculated and shown in Figure 5. The lower-order Sobol indices play more significant roles than higher-order ones. The first-order Sobol index in Figure 5A indicates that the SP1 (Pyrrole concentration), SP3 (# of EP cycles), and SP4 (# of OX cycles) have notable contributions on the sensing performance, whereas the SP2 (Cortisol concentration) and SP5 (EP scan rate) appear to be insignificant. As extremely large numbers of SP3 and SP4 completely disable the functionality of e-MIPs, SP3 and SP4 show significant impacts on sensing performance. It is important to note that while the MIP and NIP comparison study in Section 2.3 confirms the importance of cortisol's presence in the polymerization process, cortisol concentration (SP2) may play an insignificant role in the sensing performance within the investigated concentration range of 1–20 mM. Higher-order Sobol indices can be further computed to examine the multivariate contribution. The second-order Sobol index result shown in Figure 5B indicates that the combination of SP1 (Pyrrole concentration) and SP3 (# of EP cycles) is most influential to sensing performance, implying the

strong coupling between SP1 and SP3. A higher-order Sobol index with more different parameters involved generally shows a less significant influence on the sensing performance (Figure 5C and D). However, the coupling among different parameters can still be reflected. For example, while the individual SP5 (EP scan rate) is not influential, the effect of the combination of SP1, SP3, and SP5 represented by the respective third-order Sobol index is evident, which can be ascribed to their strong interrelation. The total-effect Sobol index is a more comprehensive metric for parameter importance ranking, which eventually can be obtained using Equation (S10). As shown in Figure 5E, the importance ranking in the total-effect Sobol index is quite identical with that in the first-order Sobol index, since the first-order Sobol index already accounts for the main effect.

It is worth highlighting that one main contribution of this research is to provide a generic framework, which allows one to customize the analysis where possible. For example, to better understand the impact of synthesis parameters in a more workable design space, the global analysis can be performed

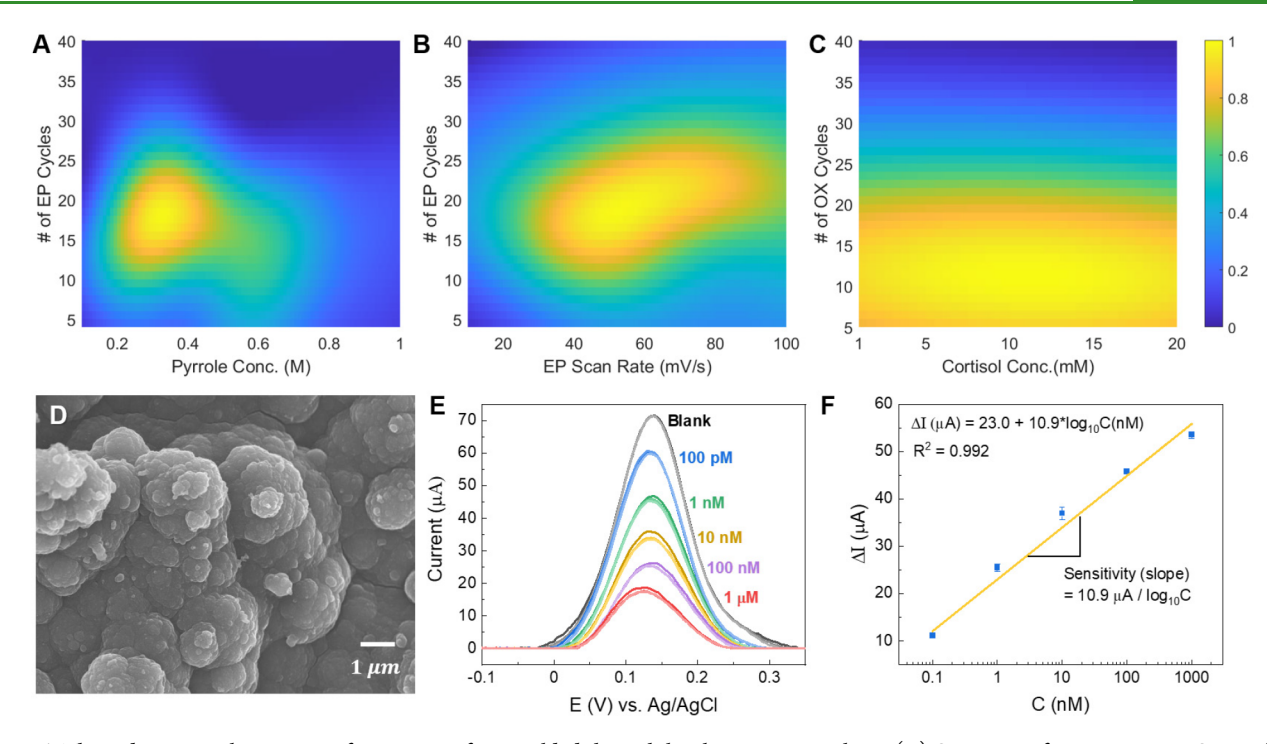


Figure 6. Three-dimensional sensing performance surfaces yielded through local sensitivity analysis: (A) Sensing performance versus SP1 and SP3 (SP2 = 10 mM cortisol, SP4 = 10 overoxidation cycles, SP5 = 50 mV/s). (B) Sensing performance versus SP3 and SP5 (SP1 = 0.32 mM pyrrole, SP2 = 10 mM cortisol, SP4 = 10 overoxidation cycles). (C) Sensing performance versus SP2 and SP4 (SP1 = 0.32 mM pyrrole, SP3 = 17 electropolymerization cycles, SP4 = 52 mV/s). (Note: the rightmost color bar represents the normalized sensing sensitivity). (D) SEM image and (E) DPV responses of the optimal e-MIP-modified SPCE to increasing cortisol concentration from 100 pM to 1 μ M in PBS with 5 mM [Fe(CN)₆]^{3-/4}. (F) Calibration curve between DPV peak current response and the logarithm of cortisol concentration with the linear regression equation.

with a narrowed design space. As excessive electropolymerization and overoxidation cycles drastically reduce e-MIPs sensing performance, SP3's and SP4's upper bounds can be intentionally reduced from 40 to 30. Following the same analysis procedures, a new set of results are obtained and shown in Figure S5. Compared to the results of the overall design space (Figure 5A), the first-order Sobol index (Figure S5A) shows the utmost significance of SP1 on e-MIPs' sensing performance and reduced impact of SP3 and SP4 as expected. In addition, the importance of the combination of SP1, SP3, and SP5 on the third-order Sobol index becomes more prominent.

3.5.2. Local Sensitivity Analysis for Synthesis Parameter Optimization. While the overall importance of synthesis parameters can be assessed using the above global analysis, the local sensitivity analysis to examine the sensing performance tendency with respect to the parameters of interest in local parametric space provides more insights behind the synthesis process to guide succeeding synthesis optimization. Following the underlying idea of local sensitivity analysis given in the Supporting Information, Note S1.3, in this research, 2 out of 5 synthesis parameters were varied along the associated dimensions of design space, and the rest were fixed to generate a 3-dimensional surface of sensing performance with respect to parameters of interest. As sample #24 shows the best sensing performance among 72 samples, the local sensitivity analysis was performed using its synthesis parameters as a starting point. As SP1 and SP3 show the strongest intercorrelation in the second-order Sobel index result (Figure 5B), the surface is generated with a fixed SP2 (Cortisol concentration) of 5 mM, SP4 (# of OX cycles) of 10, and SP5 (EP scan rate) of 50 mV/ s. As shown in Figure 6A, SP1 (Pyrrole concentration) of 0.29-0.35 M and SP3 (# of EP cycles) of 15-20 are in the optimal zone of e-MIPs synthesis, which exhibits the highest sensitivity. From the third-order Sobel index result, the combination of SP1, SP3, and SP5 (EP scan rate) exhibits the highest impact; therefore, the couplings between SP3 and SP5 are investigated at a fixed SP1 of 0.32 M pyrrole (highest point in Figure 6A). As shown in Figure 6B, the workable scan rate is from 40 to 75 mV/s, and the optimal zone is diagonal, indicating that a higher scan rate should accompany more EP cycles to achieve desired sensing performance. The predicted sensing performance is quite close in the optimal zone; therefore, 0.32 M pyrrole with 17 EP cycles at a scan rate of 52 mV/s was fixed to further examine the impact of SP2 (Cortisol concentration) and SP4 (# of OX cycles) as shown in Figure 6C. For # of OX cycles, the sensor sensitivity increases initially with each additional overoxidation scan and reaches the optimal zone between 9 and 13. After that, it starts to decrease and drops fast after the 20th cycle, which shows a great agreement with experimental observation. Figure 6C also provides the consistent observation shown in the previous Sobol index result that the cortisol concentration is the least influential parameter to sensing performance within the concentration range (1-20 mM) of interest. Nevertheless, a slight improvement in sensing performance is observed with increasing cortisol concentration. The best sensing performance is obtained when cortisol concentration is around 10 mM.

3.6. Experimental Validation of the Desired Sensor Obtained via Sensitivity Analysis. As shown in the above cross-validation result, the GPR model established has high fidelity. While the additional training data set will undoubtedly improve the model's predictive capability, the current model is

adequate to capture the overall trend of sensing performance with respect to the synthesis parameters, thus providing guidelines for synthesis optimization. It was found that the normalized sensor sensitivity of sample #24 was predicted as high as 0.908 based on the well-established GPR model. In theory, there is a better recipe that could achieve a higher normalized sensor sensitivity. Based on the local sensitivity study discussed in Section 3.5, the combination of 0.32 M pyrrole and 10 mM cortisol with 17 electropolymerization cycles at a scan rate of 52 mV/s and subsequent 10 overoxidation cycles was predicted to obtain a normalized sensor sensitivity of 0.998, which shows the improvement as compared with the best one #24 (with sensitivity 0.908) in available 72 data samples. For validation, three e-MIPs-based cortisol sensors were fabricated using this recipe, which yielded an averaged sensor sensitivity of 9.47 μ A/log₁₀C with a standard deviation of 1.30. The averaged limit of detection (LOD) is calculated to be 9.8 pM based on $3S_b/S$ (S_b : the standard deviation of 3 blank samples. S: the slope of the calibration curve). Compared with the best sensor sensitivity of $6.072 \mu A/log_{10}C$ and corresponding LOD of 20.2 pM in sample #24, 1.5-fold sensitivity enhancement was realized with a half lower limit of detection. Figure 6D-F shows the SEM image, DPV detection curves, and calibration curve of the best sensor synthesized via this recipe. The selectivity of the optimal e-MIP-modified SPCE was evaluated with common interfering species at physiologically relevant concentrations, including 5 mM lactate, 50 μ M glucose, 50 μ M ascorbic acid, 50 μ M uric acid, 50 µM acetaminophen, and 5 mM urea. As shown in Figure S6, the sensor shows no change in response after incubation with these potential interferants and a well-defined response to 1 nM cortisol, reflecting the high specificity of asprepared MIP for cortisol detection. The experimental validation result clearly demonstrates the effectiveness of the proposed framework for guiding the e-MIPs synthesis optimization. While the discrepancy of GP prediction and actual measured sensing performance of the optimized sensor does exist, the overall tendency of sensing performance with respect to synthesis parameters has been well characterized. It is worth emphasizing that the main objective of the GP model is to guide the e-MIPs synthesis optimization by suggesting the optimal synthesis parameters (inputs) instead of precisely predicting the sensitivity (output) of the e-MIPs-based sensors. To further improve the predictive capability of GP model and minimize such discrepancy, involving more data samples for model training is required.

In order to illustrate the relative location of the optimized sample in the design space, the synthesis parameters of the optimized sample and the top 10 samples with the highest sensitivities within the 72 samples are plotted in 3-dimensional graphs, as shown in Figure S7. Figure S7A,B presents these sample distributions in the test design space, where these best sensors fall in a relatively small region, with the pyrrole concentration from 0.2 to 0.4 M, # of EP cycles from 13 to 20, a scan rate of 40-75 mV/s, and # of OX cycles from 8 to 17. The only parameter with a rather spread distribution is the cortisol concentration, which is consistent with the local sensitivity analysis in Section 3.5. In the enlarged optimal design space shown in Figure S7C and D, the sample locations are randomly scattered with no clear trends with respect to sensors' sensitivity. The optimized sample locates in the optimal space, but one can hardly predict its location based on observation or human experience. This further illustrates the

importance and potential of leveraging machine learning in material design and optimization. Additionally, since the framework developed in this research is generic, it allows the synthesis optimization along with other influential factors of interest, such as the pH values. They will be subject to future research.

4. CONCLUSION

We developed an integrated data-driven framework built upon experimental data to facilitate the optimization of e-MIPs synthesis to maximize sensor sensitivity for cortisol detection. As the mainstay of the framework, the Gaussian process (GP) surrogate model with enabled probabilistic features was developed to accommodate the e-MIPs synthesis that is subject to various uncertainties. This further allows the incorporation of sensitivity analyses to explore the inherent relation between the sensing performance and synthesis parameters. Specifically, based on the global sensitivity analysis, it is found that pyrrole concentration, the number of electropolymerization CV cycles, and the number of overoxidation CV cycles are the most influential parameters for e-MIPs sensing performance. While the scan rate during electropolymerization appears less influential, it shows strong intercorrelation with pyrrole concentration and the number of electropolymerization cycles. The presence of template "cortisol" is essential in the molecular imprinting process; however, the concentration of cortisol in the investigated range (1 mM - 20 mM) appears to be the least influential. Through local sensitivity analysis, one set of optimized synthesis parameters was identified and tested by experiment. The e-MIP-based cortisol sensor fabricated by the optimized synthesis parameters outperforms the best sensor made in the original parameter samples by 1.5-fold, indicating the effectiveness of the proposed framework for guiding e-MIPs' synthesis optimization.

The concept of molecular imprinting is universal for any analytes in principle. The experimental data collected during this study can be reused. The model built can be expanded to incorporate other analytes or functional monomers by adding molecular descriptors as inputs that account for analytes' and monomers' properties and analyte-monomer interactions with corresponding experimental data as outputs. The developed methodology is also generally applicable to other sensing material development.

ASSOCIATED CONTENT

Supporting Information

The Supporting Information is available free of charge at https://pubs.acs.org/doi/10.1021/acsami.2c02474.

Methodologies in the computational framework, additional synthesis voltammograms, detection performance, and morphological characterization of representative samples, GP model's training performance, the Sobol indices over the narrowed design space, selectivity study, and the distribution of highly sensitive sensors' synthesis parameters in the design space (PDF)

AUTHOR INFORMATION

Corresponding Authors

Kai Zhou - Department of Mechanical Engineering-Engineering Mechanics, Michigan Technological University, Houghton, Michigan 49931, United States; Email: kzhou@mtu.edu

Yixin Liu – Department of Chemical Engineering, Michigan Technological University, Houghton, Michigan 49931, United States; ⊚ orcid.org/0000-0002-3758-3145; Email: yixinliu@mtu.edu

Authors

Grace Dykstra – Department of Chemical Engineering, Michigan Technological University, Houghton, Michigan 49931, United States

Benjamin Reynolds — Department of Chemical Engineering, Michigan Technological University, Houghton, Michigan 49931, United States

Riley Smith — Department of Chemical Engineering, Michigan Technological University, Houghton, Michigan 49931, United States

Complete contact information is available at: https://pubs.acs.org/10.1021/acsami.2c02474

Notes

Data Availability: The data that supports this study are available from the corresponding author upon reasonable request.

The authors declare no competing financial interest.

ACKNOWLEDGMENTS

We greatly appreciate the funding support from Michigan Technological University and National Science Foundation (Award: 2138523).

REFERENCES

- (1) Xu, J.; Miao, H.; Wang, J.; Pan, G. Molecularly Imprinted Synthetic Antibodies: From Chemical Design to Biomedical Applications. *Small* **2020**, *16* (27), 1906644.
- (2) Tarannum, N.; Hendrickson, O. D.; Khatoon, S.; Zherdev, A. V.; Dzantiev, B. B. Molecularly Imprinted Polymers as Receptors for Assays of Antibiotics. *Crit. Rev. Anal. Chem.* **2020**, *50* (4), 291–310.
- (3) BelBruno, J. J. Molecularly Imprinted Polymers. *Chem. Rev.* **2019**, *119* (1), 94–119.
- (4) Yang, B.; Fu, C.; Li, J.; Xu, G. Frontiers in Highly Sensitive Molecularly Imprinted Electrochemical Sensors: Challenges and Strategies. *TrAC Trends Anal. Chem.* **2018**, *105*, 52–67.
- (5) Moreira Gonçalves, L. Electropolymerized Molecularly Imprinted Polymers: Perceptions Based on Recent Literature for Soonto-Be World-Class Scientists. *Curr. Opin. Electrochem.* **2021**, 25, 100640.
- (6) Liu, Z.; Xu, Z.; Wang, D.; Yang, Y.; Duan, Y.; Ma, L.; Lin, T.; Liu, H. A Review on Molecularly Imprinted Polymers Preparation by Computational Simulation-Aided Methods. *Polymers (Basel)*. **2021**, 13 (16), 2657.
- (7) Cowen, T.; Karim, K.; Piletsky, S. Computational Approaches in the Design of Synthetic Receptors A Review. *Anal. Chim. Acta* **2016**, 936, 62—74.
- (8) Vamathevan, J.; Clark, D.; Czodrowski, P.; Dunham, I.; Ferran, E.; Lee, G.; Li, B.; Madabhushi, A.; Shah, P.; Spitzer, M.; Zhao, S. Applications of Machine Learning in Drug Discovery and Development. *Nat. Rev. Drug Discovery* **2019**, *18* (6), 463–477.
- (9) Pflüger, P. M.; Glorius, F. Molecular Machine Learning: The Future of Synthetic Chemistry? *Angew. Chemie Int. Ed.* **2020**, *59* (43), 18860–18865.
- (10) Gao, C.; Min, X.; Fang, M.; Tao, T.; Zheng, X.; Liu, Y.; Wu, X.; Huang, Z. Innovative Materials Science via Machine Learning. *Adv. Funct. Mater.* **2022**, 32, 2108044.
- (11) Schlexer Lamoureux, P.; Winther, K. T.; Garrido Torres, J. A.; Streibel, V.; Zhao, M.; Bajdich, M.; Abild-Pedersen, F.; Bligaard, T.

- Machine Learning for Computational Heterogeneous Catalysis. ChemCatChem. 2019, 11 (16), 3581–3601.
- (12) Yosipof, A.; Nahum, O. E.; Anderson, A. Y.; Barad, H.-N.; Zaban, A.; Senderowitz, H. Data Mining and Machine Learning Tools for Combinatorial Material Science of All-Oxide Photovoltaic Cells. *Mol. Inform.* **2015**, 34 (6–7), 367–379.
- (13) Court, C. J.; Cole, J. M. Magnetic and Superconducting Phase Diagrams and Transition Temperatures Predicted Using Text Mining and Machine Learning. *npj Comput. Mater.* **2020**, *6* (1), 18.
- (14) Muckley, E. S.; Collins, L.; Srijanto, B. R.; Ivanov, I. N. Machine Learning-Enabled Correlation and Modeling of Multimodal Response of Thin Film to Environment on Macro and Nanoscale Using "Lab-on-a-Crystal. *Adv. Funct. Mater.* **2020**, *30* (10), 1908010.
- (15) Sun, S.; Hartono, N. T. P.; Ren, Z. D.; Oviedo, F.; Buscemi, A. M.; Layurova, M.; Chen, D. X.; Ogunfunmi, T.; Thapa, J.; Ramasamy, S.; Settens, C.; DeCost, B. L.; Kusne, A. G.; Liu, Z.; Tian, S. I. P.; Peters, I. M.; Correa-Baena, J.-P.; Buonassisi, T. Accelerated Development of Perovskite-Inspired Materials via High-Throughput Synthesis and Machine-Learning Diagnosis. *Joule* **2019**, 3 (6), 1437–1451.
- (16) Mekki-Berrada, F.; Ren, Z.; Huang, T.; Wong, W. K.; Zheng, F.; Xie, J.; Tian, I. P. S.; Jayavelu, S.; Mahfoud, Z.; Bash, D.; Hippalgaonkar, K.; Khan, S.; Buonassisi, T.; Li, Q.; Wang, X. Two-Step Machine Learning Enables Optimized Nanoparticle Synthesis. npj Comput. Mater. 2021, 7 (1), 55.
- (17) Zhang, Y.; Ling, C. A Strategy to Apply Machine Learning to Small Datasets in Materials Science. *npj Comput. Mater.* **2018**, 4 (1), 25.
- (18) Hogenelst, K.; Soeter, M.; Kallen, V. Ambulatory Measurement of Cortisol: Where Do We Stand, and Which Way to Follow? *Sens. Bio-Sensing Res.* **2019**, 22, 100249.
- (19) Manickam, P.; Arizaleta, F.; Gurusamy, M.; Bhansali, S. Theoretical Studies of Cortisol-Imprinted Prepolymerization Mixtures: Structural Insights into Improving the Selectivity of Affinity Sensors. J. Electrochem. Soc. 2017, 164 (5), B3077—B3080.
- (20) Manickam, P.; Pasha, S. K.; Snipes, S. A.; Bhansali, S. A Reusable Electrochemical Biosensor for Monitoring of Small Molecules (Cortisol) Using Molecularly Imprinted Polymers. *J. Electrochem. Soc.* **2017**, *164* (2), B54–B59.
- (21) Tang, W.; Yin, L.; Sempionatto, J. R.; Moon, J.; Teymourian, H.; Wang, J. Touch-Based Stressless Cortisol Sensing. *Adv. Mater.* **2021**, 33 (18), 2008465.
- (22) Zhou, K.; Tang, J. Uncertainty Quantification in Structural Dynamic Analysis Using Two-Level Gaussian Processes and Bayesian Inference. *J. Sound Vib.* **2018**, *412*, 95–115.
- (23) Zhou, K.; Tang, J. Structural Model Updating Using Adaptive Multi-Response Gaussian Process Meta-Modeling. *Mech. Syst. Signal Process.* **2021**, *147*, 107121.
- (24) Yarman, A.; Scheller, F. W. How Reliable Is the Electrochemical Readout of MIP Sensors? *Sensors* **2020**, 20 (9), 2677.
- (25) Kroese, D. P.; Taimre, T.; Botev, Z. I. *Handbook of Monte Carlo Methods*; Wiley Series in Probability and Statistics; Wiley, 2011. DOI: 10.1002/9781118014967.
- (26) Kan, X.; Xing, Z.; Zhu, A.; Zhao, Z.; Xu, G.; Li, C.; Zhou, H. Molecularly Imprinted Polymers Based Electrochemical Sensor for Bovine Hemoglobin Recognition. *Sensors Actuators B Chem.* **2012**, *168*, 395–401.
- (27) Wang, Z.; Li, F.; Xia, J.; Xia, L.; Zhang, F.; Bi, S.; Shi, G.; Xia, Y.; Liu, J.; Li, Y.; Xia, L. An Ionic Liquid-Modified Graphene Based Molecular Imprinting Electrochemical Sensor for Sensitive Detection of Bovine Hemoglobin. *Biosens. Bioelectron.* **2014**, *61*, 391–396.
- (28) Webb, G. I.; Sammut, C.; Perlich, C.; Horváth, T.; Wrobel, S.; Korb, K. B.; Noble, W. S.; Leslie, C.; Lagoudakis, M. G.; Quadrianto, N.; Buntine, W. L.; Quadrianto, N.; Buntine, W. L.; Getoor, L.; Namata, G.; Getoor, L.; Han, X.; Jin, J.; Ting, J.-A.; Vijayakumar, S.; Schaal, S.; Raedt, L. De. Leave-One-Out Cross-Validation. In *Encyclopedia of Machine Learning*; Springer US: Boston, MA, 2011; pp 600–601. DOI: 10.1007/978-0-387-30164-8 469.

- (29) Support Vector Machines: Theory and Applications; Wang, L., Ed.; Studies in Fuzziness and Soft Computing; Springer Berlin Heidelberg: Berlin, Heidelberg, 2005; Vol. 177. DOI: 10.1007/b95439.
- (30) Grąbczewski, K. *Meta-Learning in Decision Tree Induction*; Studies in Computational Intelligence; Springer International Publishing: Cham, 2014; Vol. 498. DOI: 10.1007/978-3-319-00960-5.
- (31) Aggarwal, C. C. Neural Networks and Deep Learning; Springer International Publishing: Cham, 2018. DOI: 10.1007/978-3-319-94463-0.
- (32) Liu, Y.; Zhou, K.; Lei, Y. Using Bayesian Inference Framework towards Identifying Gas Species and Concentration from High Temperature Resistive Sensor Array Data. *J. Sensors* **2015**, 2015, 1–10.

□ Recommended by ACS

Enabling the Selective Detection of Endocrine-Disrupting Chemicals via Molecularly Surface-Imprinted "Coffee Rings"

Jihye Lee, Suck Won Hong, et al.

FEBRUARY 22, 2021 BIOMACROMOLECULES

READ 🗹

Photopolymerization and Photostructuring of Molecularly Imprinted Polymers

Ernesto III Paruli, Carlo Gonzato, et al.

SEPTEMBER 30, 2021

ACS APPLIED POLYMER MATERIALS

READ 🗹

Toward Rational Design of Electrogenerated Molecularly Imprinted Polymers (eMIPs): Maximizing Monomer/Template Affinity

P. U. Ashvin Iresh Fernando, Lee C. Moores, et al.

AUGUST 20, 2021

ACS APPLIED POLYMER MATERIALS

READ 🗹

Probing Peptide Sequences on Their Ability to Generate Affinity Sites in Molecularly Imprinted Polymers

Elena V. Piletska, Sergey Piletsky, et al.

DECEMBER 12, 2019

LANGMUIR

READ 🗹

Get More Suggestions >